View metadata, citation and similar papers at core.ac.uk
brought to you by CORE
provided by Universidade do Minho: RepositoriUM

Heterozygous deletion of the Williams-Beuren syndrome critical interval in mice recapitulates most features of the human disorder

Maria Segura-Puimedon[1,2], Ignasi Sahún[3], Emilie Velot[4], Pierre Dubus[5], Cristina Borralleras[2,6], Ana J. Rodrigues[7], María C. Valero[8], Olga Valverde[1,6], Nuno Sousa[7], Yann Herault[4], Mara Dierssen[2,6,9], Luis A. Pérez-Jurado[1,2,6], Victoria Campuzano[1,2,6,*]

[1]Departament de Ciències Experimentals i de la Salut, Universitat Pompeu Fabra, 08003 Barcelona, Spain

[2]Centro de Investigación Biomédica en Red de Enfermedades Raras (CIBERER), ISCIII, Spain

[3]Laboratory Animal Applied Research Platform (PRAAL) 08028 Barcelona, Spain

[4]Institut de Génétique et de Biologie Moléculaire et Cellulaire, Department of Translational medicine and Neuroscience, Centre National de la Recherche Scientifique, CNRS UMR7104, Institut National de la Santé et de la Recherche Médicale, INSERM U964, Université de Strasbourg, Institut Clinique de la Souris, ICS, PHENOMIN, GIE CERBM, 67404 Illkirch CEDEX / France

[5]EA2406, University of Bordeaux, Bordeaux, France

[6]Neurosciences Program, Institut Hospital del Mar d'Investigacions Mèdiques (IMIM), 08003 Barcelona, Spain

[7]Life and Health Sciences Research Institute (ICVS), University of Minho, Braga, and ICVS/3B's – PT Government Associate Laboratory, Braga/Guimarães, Portugal

[8]Department of Entomology, University of Illinois, Urbana Champaign, IL 61801, USA

[9]Centre de Regulació Genòmica (CRG), 08003 Barcelona, Spain

[*]Corresponding author: Victoria Campuzano PhD. Unitat de Genètica. IMIM-Institut Hospital del Mar d'Investigacions Mèdiques .Aiguader 88, 08003 Barcelona, Spain, FAX: 34 93 3160901, Telephone: 34 93 3160855, e-mail: victoria.campuzano@upf.edu

© The Author 2014. Published by Oxford University Press. All rights reserved. For Permissions, please email: journals.permissions@oup.com

Abstract

Williams-Beuren syndrome is a developmental multisystemic disorder caused by a recurrent 1.55-1.83 Mb heterozygous deletion on human chromosome band 7q11.23. Through chromosomal engineering with the cre-loxP system, we have generated mice with an almost complete deletion of the conserved syntenic region on chromosome 5G2. Heterozygous complete deletion mice were viable, fertile, and had a normal lifespan, while homozygotes were early embryonic lethal. Transcript levels of most deleted genes were reduced 50% in several tissues, consistent with gene dosage. Heterozygous mutant mice showed postnatal growth delay with reduced body weight and craniofacial abnormalities such as small mandible. The cardiovascular phenotype was only manifested with borderline hypertension, mildly increased arterial wall thickness, and cardiac hypertrophy. The neurobehavioral phenotype revealed impairments in motor coordination, increased startle response to acoustic stimuli and hypersociability. Mutant mice showed a general reduction in brain weight. Cellular and histological abnormalities were present in the amygdala, cortex and hippocampus, including increased proportion of immature neurons. In summary, these mice recapitulate most crucial phenotypes of the human disorder, provide novel insights into the pathophysiological mechanisms of the disease such as the neural substrates of the behavioral manifestations, and will be valuable to evaluate novel therapeutic approaches.

INTRODUCTION

Williams-Beuren syndrome (WBS, MIM 194050) is a rare neurodevelopmental disorder with an incidence of 1/7500 newborns, which usually occurs sporadically (1). It is caused by the hemizygous deletion of 26-28 contiguous genes on chromosome band 7q11.23 (2, 3) . The 1.55 Mb common deletion (90% of the patients) is mediated by meiotic non allelic homologous recombination between misaligned large region-specific segmental duplications that flank the WBS critical region (WBSCR) (4, 5).

WBS patients have specific dysmorphic features due to craniofacial abnormalities, mild growth retardation, and a generalized arteriopathy characterized by supravalvular aortic stenosis and hypertension, other connective tissue alterations and occasional hypercalcemia (6, 7). Patients also present mild to moderate intellectual disability, hyperacusia, mild hypotonia and motor problems, and a characteristic cognitive profile including hypersociability and deficient visuospatial abilities (8-11). Neuroimaging and electrophysiological studies have revealed reduced brain volume along with structural and functional abnormalities in many brain areas, especially in regions related to the social phenotype (amygdala, insula and orbitofrontal cortex), or to the visuospatial alterations (hippocampus and retina) (12, 13).

Based on clinical-molecular correlations in a few atypical patients with partial deletions, *GTF2I* (MIM 601679) and *GTF2IRD1* (MIM 604318) are strong candidate genes for the craniofacial and most neurobehavioral features of WBS, while *ELN* (MIM 130160) is the major player in the cardiovascular phenotype with *NCF1* (MIM 608512) as a relevant modulator (14-16). However, although the majority of individuals with WBS have almost identical deletions, they do show significant phenotypic differences. These may be attributed to variation in the non-deleted alleles on the normal chromosome 7 and/or to alleles at modifier loci located elsewhere in the genome. Therefore, given the incomplete penetrance of some features, attempts to resolve the gene/function relationship by studying single individuals with unusual smaller deletions are considered problematic, especially if a lacking phenotype is attributed to genes that are not deleted (17, 18).

In mouse, the entire WBSCR is conserved on chromosome band 5G2 in reverse orientation with respect to the centromere and the flanking genes (19, 20). Several mouse models have been generated including the single-gene knock-out of some deleted loci, although relevant phenotypes in heterozygous knock-out animals were only evident in six models: *Baz1b*, *Cyln2, Gtf2i*, *Gtf2ird1, Eif4h and Eln* (18, 21-25). There are also mice with partial (approximately half) deletions of the critical interval, the proximal deletion (PD) and distal deletion (DD), and a double heterozygote (D/P) created by crossing animals with the two partial deletions. D/P mice are deleted for the entire WBSCR but the two half deletions are *in trans* with a homozygous loss of *Limk1* (26). All these animals have provided relevant insights into the specific contribution of several genes to the WBS phenotype, but do not carry the same molecular defect present in humans.

Here we present a mouse model that mimics the most common deletion found in WBS patients, with the heterozygous loss of the entire single-copy genomic region between the *Gtf2i* and *Fkbp6* genes. These complete deletion (CD) mice recapitulate most physical and cognitive features present in WBS patients, becoming an optimal model to unravel the molecular mechanisms of the disease as well as to evaluate novel therapeutic approaches.

RESULTS

Generation of a mouse model with complete deletion of the WBSCR

LoxP sites were inserted by two subsequent steps of homologous recombination at the two target locations in ES cells: the first one replacing exon 2 of the *Gtf2i* gene (24) , and the second one within intron 5 of the *Fkbp6* gene (Fig. 1A). We then selected single ES clones with both loxP sites. Verification of the single integration and the location of the two loxP sites either in *cis* or in *trans* was performed by FISH with a probe for the *HPRT* cassette (Fig. 1B). Clones with the 2loxP sites in *cis* were electroporated with a Cre-recombinase expressing vector, and positive deleted clones (ESSP9) were selected and the genotype was confirmed by MLPA (Fig. 1B).

CD mice were then obtained following two strategies. Both, 1) ESSP9 cells with the deletion and 2) ES cells with the 2loxP sites *in cis* were injected into blastocysts to obtain chimeric mice. A chimeric male derived from ESSP9 and the other from 2loxP ES cells, transmitted the modified allele through the germline. CD mice were directly obtained in the offspring of the chimeric ESSP9 male. To complete the second strategy, 2loxP mice were mated with TgPGK-Cre mice expressing Cre-recombinase, to directly obtain CD mice in the offspring. The offspring genotype was determined by MLPA in all cases.

In order to validate the functional consequences of the deletion in heterozygous CD mice, we demonstrated a reduction of the expression of all 7 WBSCR genes tested by qRT-PCR of RNA from several tissues, with levels ranking between 20–75% relative to wild-type (WT) littermates and consistent with heterozygous loss (Fig.1C).

Viability, somatic growth and connective tissue phenotypes

Segregation of heterozygous CD when crossed with WT followed the expected Mendelian ratios (Supplementary Material, Table S1). However there was a significant decrease in the number of pups per litter between embryos (E12.5-E18.5) and weaned animals ($P \leq 0.001$), with a trend toward greater loss of CD animals (Supplementary Material, Table S1 and Fig. S1A). Although fertility was not compromised in CD animals of any gender, we observed a significant reduction ($P=0.008$) in the number of pups per litter in CD females respect to WT females (Supplementary Material, Table S1). When heterozygous intercrosses were performed, no homozygous CD mice were obtained or even detected as early as 9.5 days post coitum, which was expected given the reported lethality of the homozygous knock-out of at least two single genes of the interval, *Eln* and *Gtf2i* (23, 24, 27).

WBS patients usually present mild growth retardation of prenatal onset maintained into adulthood, and 70% of them have final statures below the 3rd percentile for mid parental height (28).

Connective tissue abnormalities such as hernias, diverticulosis of gut and bladder and rectal prolapse are common (29). CD animals did not show a reduction in the body weight at birth, but it was significantly deceased already in the first month and maintained until two years of age, with a more accused difference in males ($F_{1,19}$=53.069, $P \leq 0.001$) than in females ($F_{1,18}$=22.539, $P \leq 0.001$) (Supplementary Material, Fig. S1B). The macroscopic study of several tissues showed no differences in the general tissue organization at 16 weeks old.

Lifespan was normal in CD animals. All mice died between 28 and 32 month (Supplementary Material, Fig. S1C), and no differences were found between groups with respect to death causes, mainly being tumors such as lymphoma B (follicular type) in both genders and genotypes, which is common in the C57BL/6 background. Although differences did not reach significance, a wider variety of tumors and a higher prevalence of steatosis were observed in the CD animals (Supplementary Material, Table S2).

Ten independent cultures of mouse embryonic fibroblasts were established from 10.5-12.5 days post-coitum embryos and characterized following the 3T3 protocol. No differences were observed between CD and WT fibroblast regarding the immortalization passage, growth, or saturation curves (Supplementary Material, Fig. S2).

Mild cardiovascular phenotype

Haploinsufficiency for *ELN* is responsible for the generalized arteriopathy highly penetrant in WBS patients, also present in heterozygous mice for *Eln* knock-out or deletion of the distal half of the WBSCR interval, characterized by arterial wall thickness and luminal narrowing in some arteries, and manifested by hypertension and other cardiovascular complications (23, 30). Cardiovascular defects have also been described in heterozygous and knockout mice for *Baz1b* (25).

A significant increase in the mean arterial pressure was found in the CD mice respect to WT littermates (*P*=0.032) (Supplementary Material, Fig. S3A). Autopsies at 32 weeks of age revealed a mild increase in the aortic wall thickness and the number of lamellar units (Table 1; Supplementary Material, Fig. S3B and C). Heart size of CD animals, measured by heart wet-weight relative to the body weight, was evaluated at different ages. Significant cardiac hypertrophy was found both in young (3-4 months) or old animals (9-12 months) ($P \leq 0.001$) (Supplementary Material, Fig. S3D). This cardiovascular phenotype did not affect lifespan of CD mice and was significantly milder than the phenotype of other models with *Eln* deletion, such as the DD mice (Supplementary Material, Fig. S3) (30). Given that *NCF1,* encoding the p47phox subunit of the NADPH oxidase, has been described as a modulator of blood pressure and the cardiovascular phenotype in WBS patients and DD mouse models (14, 16), we studied the expression levels of *Ncf1* in different tissues of the CD mice by qRT-PCR. In contrast to DD mice that showed a two-fold overexpression, *Ncf1* expression in CD animals was average in heart and liver and even decreased in the aorta (Supplementary Material, Fig. S3E).

Craniofacial features and smaller mandibles

The characteristic facial features of WBS individuals include frontal narrowing, flat nasal bridge, periorbital fullness, malar flattening, a short up-turned nose with anteverted nostrils, a long flat philtrum, full cheeks, prominent lips, a wide mouth and a small chin, which allow the clinical diagnosis and can also be defined by three-dimensional imaging (31). Analysis of computed tomography (CT) cranial scans in partial deletion mouse models suggest that haploinsufficient genes in the DD deletion contribute primarily to shorter skulls (26) although relevant craniofacial features were also observed in knock-out mice for the *Gtf2i* ,*Gtf2ird1*, *Baz1b* and *Eif4h* genes (18, 21, 24, 32)

A morphometric analysis of the cranial structure was performed following CT scans of the head of CD and WT littermate females, with ulterior reconstruction of 3D skull images using 39 cranial and

22 mandible landmarks. No global differences in the size of the skull were observed, although a tendency to smaller nose was observed in CD females (Fig. 2A and B), along with a significantly reduced mandible (*P* =0.028) (Fig. 2C and D). Regarding shape, no global differences were evident but there was a clear tendency for a flatter nose in CD mice (Supplementary Material, Fig. S4).

Reduced brain size and reduced number of YFP-expressing pyramidal neurons

Both global and regionally specific differences in brain anatomy have been described in WBS (33), including reduced total brain volume affecting more the white (~18%) than the grey matter (~11%) (34). Differences in volume/morphology affect the amygdala, cortex, cerebellum, corpus callosum, hippocampus, and thalamus (13, 35-39). In addition, increased neuronal packing density has been observed in primary visual cortex (40). Genes deleted in the DD mice have been proposed to affect overall brain growth, while genes in the PD are associated with increased neuronal packaging in the somatosensory cortex (26).

Brain weight was reduced in CD mice by around 9%, both in males and females (P <0.001) (Fig. 3A), which was proportional to the reduced body weight at the same age (9-11% in males and 8-13% in females). Histological analyses did not reveal any major alterations of brain structures. We then performed a more precise volumetric and cytological structural analysis of several brain regions in CD males. In the amygdala, although the volume was preserved (Supplementary Material, Fig. S5A), we observed a general decrease in cell density, significant in the basolateral area (P=0.029) (Fig. 3B). Preliminary results in cell type distribution in this particular area, suggest that the observed reduction in cell density could be due, in part, to a reduction in GFAP$^+$ cells (Supplementary Material, Fig. S5B).

In the hippocampus, there was a significant volume reduction in the CA3 stratus oriens and stratus pyramidalis regions (*P* =0.016) (Fig. 3C). No differences were found in cell density in any compartment (Supplementary Material, Fig. S5B). However, immature neural density analyzed by doublecortin immunostaining in the subgranular zone of dentate gyrus (DG) from adult males, was significantly increased in CD respect to WT (*P* =0.006) (Fig. 3D). Preliminary results in neural morphology of hippocampus suggest a reduction in the dendritic length of CD mice compared to WTs (*P*=0,023) (Supplementary Material, Fig. S5C). Similarly, a reduction in the spine density in the apical oblique zone was observed in CD males (*P*<0,001) (Supplementary Material, Fig. S5D). At the orbitofrontal cortex, neither volume nor cell density were different between CD mice and WT littermates (Supplementary Material, Fig. S6A and B).

In addition to the morphological differences already described, we observed a remarkable and unexpected reduction in the number of YFP$^+$ pyramidal cells in CD males relative to WT littermates (Fig. 4A). We quantified the percentage of YFP$^+$ pyramidal cells in three areas (motor and somatosensory cortex and hippocampal region CA1) as a fraction of all fluorescent Nissl-stained neurons (Fig. 4B). In all three regions CD males had a drastic reduction of YFP$^+$ neurons. The fraction of YFP$^+$ neurons was decreased by 88% in motor and somatosensory cortex, and by 82% in CA1 (Fig. 4C; $P \leq 0.001$ in all pairs). The reduction in motor cortex occurred in contrast to the higher neuronal density (16.46%; *P*=0.009) observed with the Nissl-staining. Therefore, this reduction of YFP$^+$ cells does not correspond to the total number of cells and could result from overall down-regulation of YFP expression or transgene silencing in many cells of CD animals. In cortex, significant lower number of YFP$^+$ cells in mutant was present as early as P12-14 developmental stage (*P*=0,036), and nearly significant reduction was observed in hippocampus (*P*=0,057) (Fig 4D), suggesting that the reduced number of YFP$^+$ neurons in mutant mice results from transgene silencing.

In summary, the size reduction with subtle changes in cell density of several brain regions, the increased Dcx-staining in DG and the reduced number of YFP$^+$ cells point to a less mature brain with deficiencies in establishing or maintaining neuronal subpopulations in CD mice.

Cognitive and behavioral phenotype

A general behavioral characterization, including neurosensorial, motor, learning and attention tests, was performed in CD mice to determine the characteristics shared with human patients and other mouse models.

Motor function and exploratory activity

Motor problems along with hypotonia and some cerebellar signs are present in WBS patients (9). Mice with partial WBSCR deletions (PD and P/D) also showed poor performance on the rotarod test indicative of motor problems (26).

In an initial approach to the motor phenotype of CD males, we observed significant deficit in the motility tonus strength (*P*=0.002) (Fig. 5A). However, no differences were obtained in gait and equilibrium. We performed open-field test to analyze the exploratory activity and anxiety. There were no significant differences in activity, as measured by the distance travelled, as well as in anxiety-like behavior, as measured by the total distance travelled in the center of the arena, as compared to WT littermates. To further analyze possible motor coordination problems, we assessed the accelerating rotarod test finding a significant reduction in the latency to fall in CD mice that started as early as 7 rpm (Fig. 5B).

Acoustic startle reflex

The majority (85–95%) of individuals with WBS are reported to show hyperacusia or odinoacusia, being clearly hypersensitive to certain types of noise (41). In order to test this phenotype in mice, we studied the startle response to sudden noise. We could see a significantly increased startle response in CD mice at 120 dB, suggestive of hyperacusia or odinoacusia as in human WBS (Fig. 5C).

Learning and memory

People with WBS exhibit developmental delay and cognitive impairment, usually in the mild to moderate range (42), along with significant deficits in visuo-spatial constructive cognition (43).

Fear conditioning is a behavioural paradigm in which animals learn to predict aversive events (44). A slight reduction in the freezing time after the conditioning stimulus was found in CD mice consistent with impaired fear memory performance (Supplementary Material, Fig. S7A).

The novel object recognition test is a visual discrimination test for memory and attention. No significant differences were observed among the two genotypes (Supplementary Material, Fig. S7B).

In a visuo-spatial learning acquisition paradigm, the Water Maze test (WM), mice have to form an allocentric map to find the position of a hidden platform during several acquisition sessions, helped by external cues around the pool. No differences were found concerning latency to escape in pre-training or acquisition sessions (Supplementary Material, Fig. S7C). Significant differences were found in pre-training (*P*=0.045), and in the first acquisition sessions (A2: *P*=0.011; A3: *P*=0.021) regarding the distance and average speed (Fig. 6A and B). CD mice travelled less distance and swam slower than WT mice during the first sessions even though no differences in escape latency were noticed. Both groups comprehended the platform localization with no differences in the time spent in the four different quadrants during acquisition sessions (Supplementary Material, Fig. S8A). In the probe session (Removal) CD mice travelled more distance across the trained quadrant (NE) than WT mice (*P*=0.069) and significantly less (*P*=0.047) in the adjacent quadrant (NW) (Fig. 6C), suggesting an improvement in memory probably due to an increase in the persistence of the learning done. No vision or motor impairment was observed when guided session (Cued) was analyzed. When Reversal session was analyzed, in which we evaluate cognitive flexibility, both groups showed the same escape latency (Supplementary Material, Fig. S8B). However, a significant reduction in swimming speed was observed in CD mice in reversal session 1 (*P*=0.025) and in reversal session 2 (*P*=0.037, Fig. 6D). On the other hand, significant differences were shown in the time spent in the center or the periphery of the pool in acquisition sessions, cued session and both reversal sessions. CD animals showed a reduced thigmotaxic behavior spending more time in the center of the pool (Supplementary

Material, Fig. S8C). Finally, a deeper analysis of the learning strategy performed by animals through the analysis of Gallagher (average distance to the platform) and Whishaw (percentage of time in a direct corridor to the platform) index was performed. A trend of a better searching strategy with a reduced distance and an increased permanence in the direct path to the platform were showed in CD mice (Supplementary Material, Fig. S8D).

Social behavior

Individuals with WBS have inappropriate social approach behavior, do not show stranger-anxiety as children and continue to display overly social and outgoing behavior towards strangers as adults (45).To explore sociability in the CD mice, we performed an adaptation of a social approach/interaction test previously described (46). WT mice exhibited a habituation effect, exploring the novel mouse for less time during the second 5-minute segment than during the first period of time (P=0.007). By contrast, CD mice showed less habituation with no significant difference in the amount of time spent investigating the unfamiliar mouse during the first and second 5-minute segments (P=0.101) (Fig. 7A). The time spent in nose-to-cage contact by approach to the cage was significantly increased in CD respect to WT littermate males (RS1, P=0.003 and RS3, P=0.004) (Fig. 7B). Total interacting time with the first novel mouse showed a significant difference between WT and CD mice (P=0.001) (Fig. 7C), mainly due to the lesser habituation in sessions 2 and 3 (Fig. 7D). In the fourth and last trial, the subject was allowed to interact with another novel mouse. As expected for a social interest an increase in the interaction time was observed in both genotypes (Fig. 7D).

DISCUSSION

WBS is a widely studied complex neurodevelopmental disorder with a specific combination of physiological and cognitive deficits, caused by a recurrent heterozygous deletion of contiguous genes on human chromosome band 7q11.23 (47). Several strategies have been followed in order to dissect the molecular mechanisms underlying the disease, including the generation of animals with single gene knock out as well as partial deletions of the critical interval. To better achieve all these goals we have created for the first time a mouse model that mimics the most common deletion found in human patients.

The CD mouse model showed reduced body weight, not significant at birth but slightly progressive during postnatal growth, being ~20-30% smaller than littermates at 20 months of age, which is a similar pattern to the growth delay present in human patients. Fertility was not affected, but CD females had lower number of pups per litter in general, and homozygosity for the CD deletion was lethal early in embryogenesis. Regarding survival, there were no significant differences between CD and WT animals, as it has been reported in other published partial mouse models for WBS (6, 26). The most common cause of death in CD animals was the development of lymphomas, similar to WT animals of the C57BL/6 background (48). However, a wider variety of tumors was identified in CD mice, including lung carcinoma, histiocytic sarcoma and myeloproliferation .

Cardiovascular manifestations are one of the hallmarks of WBS present in ~85% of patients, particularly a generalized arteriopathy with luminal stenoses of large arteries, mostly supravalvular aortic and/or pulmonary stenoses, and leading to hypertension in >50% of patients (49). A decreased amount of elastin protein due to *ELN* gene haploinsufficiency causes developmental anomalies with a poor structure of the elastic lamellae, increased arterial wall thickness and vascular narrowing, which is thought to evolve by chronic activation of the NADPH complex producing oxidative stress (50). Deletion of *NCF1*, coding for the p47phox subunit of the NADPH complex, has being shown to modify the cardiovascular phenotype by decreasing oxidative stress in WBS and in the DD mouse model (14, 16). CD mice presented a mild increase in the arterial wall thickness and disorganization of the elastin sheets, manifested with mild hypertension at 32 weeks of age and cardiac hypertrophy in autopsied animals. All these phenotypes were milder in CD mice compared with DD mice, and similar to the D/P model, whose reported increase in the arterial pressure was 10.1% at the same age (30). *Eln* gene expression was reduced in all tissues tested of the CD mice including the heart. However, *Ncf1* gene expression in CD was comparable to the WT or even reduced in aortic tissue. These results further indicate that reduced expression of *Ncf1* can ameliorate the cardiovascular manifestations and hypertension associated with the elastin arteriopathy of WBS (16). Given that the *Ncf1* gene is intact, it is still unclear how the CD deletion, similar to the PD deletion, can affect *Ncf1* gene expression, most likely by removing a cis-acting regulatory element.

A characteristic facial appearance is present in all WBS patients, with flat midface and short upturned nose, retrognathic or a micrognathic mandible, as well as definite cranial abnormalities with a shortened cranial base (47, 51, 52) . A shorter skull was present in the DD and D/P mouse models, mostly at the posterior and occipital cranial bases (26). *Baz1b* is strongly expressed in the mesenchyme of the maxillary and mandibular prominences, branchial arch 2 and the nasal processes (32) and abnormal nose was also reported in single gene knock-out of the *Gtf2i* and *Gtf2ird1* genes (18, 24). We did not see large differences in the skull of CD females but a tendency to a smaller and flatter nose was present along with a smaller mandible, which could recapitulate the flat midface and micrognathic chin of the human patients. First insights in the neuroanatomical phenotype of WBS came from studies reporting an 11-13% reduction in the brain volume (36, 40). Moreover, multiple abnormalities both structural and functional have been observed in different brain areas of human patients, especially in the amygdala, the orbitofrontal cortex and the hippocampus, among others (12, 34, 53, 54). CD mice recapitulate the reduction in brain weight with an 11% decrease in males and 7% in females. Consistent with the brain weight reduction, a general volume reduction was appreciated in all studied areas in CD animals, similar to the anomalies detected in DD and P/D males but not the PD males (26). The heterozygous deletion generated in CD mice also led to a reduction in both the dendritic length and the spine density in the hippocampus. We also found a remarkable reduction (by 81-87%) of YFP-expressing cells in several brain regions of CD mice. In both genotypes, we found individual YFP$^+$ neurons as early as P9. By P12-14, the number of YFP$^+$ neurons increased in WT, but remained low in CD mutants, suggesting that the reduced number of YFP$^+$ neurons in mutant mice results for transgene silencing. Similar findings have been previously described in a mouse model for another neurodevelopmental disorder, Rett Syndrome, caused by *Mecp2* knock-out (55). More studies are needed to define whether the reduced number of YFP$^+$ neurons correlates with actual alterations in the proportion of certain subclasses of pyramidal neurons or it is due to aberrant developmental activation of the YPF transgene in CD mice. The hippocampus presents functional abnormalities in humans with reduced blood flow and synaptic activity (12), which could be related with the general reduction of volume in CA3 stratus oriens and stratus pyramidalis, and increased number of immature neurons found in the CD model.

The amygdala is essential for social cognition, fear conditioned learning and anxiety processing. Studies in WBS individuals have provided controversial results, reporting either preservation or increase amygdalar volume as well as increased reactivity (12, 54). A reduction of the freezing behavior in the fear conditioning test was present in CD animals. The same tendency to a reduction in fear conditioning was observed in the D/P model, although significance was only achieved in the DD model, indicating a possible compensatory role of the PD region in the test (26). Interestingly, studies with rats presenting lesions in the basolateral amygdala showed a reduction in the freezing time (56) and studies in humans go in the same direction, pointing to a possible relation of the obtained results with the significant reduction in the number of cells of the basolateral amygdala in the CD model. Regarding learning and attention the water maze test did not reveal visuo-spatial deficits in the CD mice but differences in acquisition, speed or reversal sessions. Interestingly, significantly different thigmotaxic behaviour was found in the CD model, spending more time in the center of the pool, which could be related to the uninhibited and anxiety-like behaviors found in human patients. However, we could not find anxiety-like behavior in the open field test in CD mice, as reported in the D/P and PD models (26).

Social disinhibition represents the most unique and intriguing behavioral characteristic of individuals with the WBS deletion. It has been proposed that WBS patients do not recognize social features such as facial expression, leading to hypersociability (6). In a direct social interaction test, PD mice displayed more bouts of active social interactions relative to the other genotypes (26) and *Gtf2i* heterozygous animals showed lack of habituation (46). In the paradigm we used, CD animals exhibited increased social interactions, spent more time with unfamiliar animals, and did not easily habituate to repeated stimuli retaining social interest. Both WT and CD animals recovered their interest in the last session, when a new animal was exposed. Our results suggest that the observed phenotype in CD animals is due to increased sociability rather than memory problems and the lack of habituation may be caused by impaired recognition of social partners. Also, hypersociability involves increased social interactions, in addition to less social anxiety which could explain the less social dominance observed by others in tube paradigm (26).

Finally, a significant increase in the startle response to noisy stimuli, suggestive of hyperacusia or odinoacusia, was found in CD mice. Although no differences using this test were reported in the D/P and DD mice, a significant increase was also found in the PD and *Gtf2i* mice (26).

In summary, the CD mouse is the first mouse model presenting the most common WBS deletion. These animals recapitulate most of the phenotypes present in the human WBS disorder, except for a mild cardiovascular phenotype, which reinforces the previously reported pathogenic mechanism implicating *Ncf1* function in modulating severity mediated by oxidative stress. The CD model shows a reduced body and brain weight, characteristic changes in several brain regions, motor and social alterations and specific behavioral changes related to the human patients. This model will be useful for future studies to deepen into the pathophysiological mechanisms of the disease such as the neural substrates of the behavioral manifestations, and will be valuable to evaluate novel therapeutic approaches.

MATERIALS AND METHODS

The study has been performed in accordance with the ARRIVE guidelines, reporting of in vivo experiments (http://www.nc3rs.org/ARRIVE).

Ethics statement

Animal procedures were conducted in strict accordance with the guidelines of the European Communities Directive 86/609/ EEC regulating animal research and were approved by the local Committee of Ethical Animal Experimentation (CEEA-PRBB). All mice were bred on a majority C57BL/6J background (97%). Tail clipping was performed within 4 weeks of birth to determine the genotype of each mouse using MLPA and appropriate primers (Supplementary Material, Table S3).

Generation of the CD mice

Fkbp6 genomic sequences were cloned by plate hybridization from a lambda genomic library. For insertion of a loxP site in the intron five of *Fkbp6* we subcloned upstream and downstream genomic fragments in a plasmid containing the PGK-hygro cassette. The resulting final targeting vector, p936, was linearized and electroporated into mouse G6 ES cells (24) (Fig. 1A), and recombinant clones were selected in the presence of Hygromycin. Positive 2loxP clones were screened for correct homologous recombination by Southern blot using an external probe that recognizes an 11Kb WT and 5.2 Kb homologous recombinant EcoRI bands. We used FISH analysis to select clones with *in cis* integration of both cassettes using HPRT cassette as probe. To obtain ES cell clones that carry the complete deletion, we introduced Cre-recombinase into 2loxP clones and selected for neo_S and $puro_R$ ES cell colonies. Positives clones were genotyped by MLPA. The mix probes used were *Cult-1* and *Wbscr17* as external genes and *Gtf2i, Limk1, Cyln2, Fkbp6*, *Baz1b* and *Rcf2* as genes inside the deletion (Fig. 1B). WBSCR complete deleted clone ESSP9 was chosen for the analysis.

Both 2loxP and 1loxP ES cells were injected into blastocysts from strain C57BL/6J and several chimeric mice were obtained. One male chimera each, derived from 1loxP and 2loxP ES cells, transmitted the modified allele through the germline. 2LoxP mice were crossed with C57BL/6 mice expressing the Cre-recombinase early in development until recovery of CD offspring. In both strategies, first mice with the deletion in germinal line were considered F0 and submitted to genotyping by MLPA to confirm the deletion. CD mice were subsequently backcrossed with C57BL/6 until F9 generation, genetic background present in all animals studied in this work (B6.129S8-Del(5Gtf2i-Fkbp6)1Vcam/Vcam, MGI: 5555958).

To look for fluorescence pyramidal neurons we mated heterozygous CD mice (males and females) with Thy1-YFP transgenic mice (B6.Cg-Tg(Thy1-YFPH)2Jrs/J, Jackson Laboratory)(57).

Mouse embryonic fibroblasts characterization

Mouse embryonic fibroblasts (MEFs) were obtained following a previously described protocol. Spontaneous immortalization was carried out following a classical 3T3 protocol (58). Cell line characterization followed the established protocols (59) including immortalization, growth curve and saturation rate.

Gene expression analyses

mRNA was extracted from several mouse tissues using TRIZOL reagent (Invitrogen, Carlsbad, CA, USA). To perform quantitative reverse transcribed (RT)-PCR analysis 2 μg of mRNA were used for first-strand cDNA synthesis with Superscript II (Invitrogen). Primers were designed to amplify products that span an intron in all cases using the Primer3 software Version 0.4.0 (60) (Supplementary Material, Table S3). Real-Time PCR was performed using the SYBR Green Ready Master Mix according to the manufacturer's instructions in an ABI PRISM 7900HT Sequence Detection System (Applied Biosystems). The standard curve method was used for the analysis. The results were normalized respect to a housekeeping gene selected for its stable expression among the different tissues. A reagent-only (no DNA) negative control sample was always included in each run.

Experiments were performed a minimum of 3 times in 384-well plates with three replicates per sample. Raw data was obtained using SDS 2.3 software (Applied Biosystems).

Growth and survival curves

A total of 11 WT and 10 CD male animals, 16 WT and 16 CD female mice were used for growth curves. Weight was recorded every month, from 1st to 22nd months of age. 10 females and 12 males from each WT and CD groups were used for survival curves. Animals were recorded daily and sacrificed under the human endpoint criteria. Organs were collected when possible for histopathology.

Blood pressure measurements and heart histopathology

Systolic, mean, and diastolic blood pressure were measured in conscious male mice on three separate occasions by using a tail cuff system (Non-Invasive Blood Pressure System, PanLab), as previously described (24). For heart histopathology, mice were sacrificed at 16-week-old. The analysis of heart weight, wall thickness and lamellar units were performed as previously described (24).

Craniofacial analysis

Craniums were obtained from 15 CD and 15 WT females and stored in 100% ethanol. We only used females in order to avoid the use of a greater number of animals. 3D coordinates of 39 cranial and 22 mandible relevant landmarks were recorded using Landmark software and posterior comparisons were performed using the Euclidean distance matrix analysis (EDMA) with the software WinEDMA (version 1.0.1 beta). 3D data were converted into linear distances compiling into a matrix. Both the form difference matrix (FDM) and the size difference matrix (SDM) were analyzed. A ratio different from 1 (FDM) or 0 (SDM) for any linear distance indicates that the two samples are not similar for that measure.

Confidence intervals were estimated using a non-parametric bootstrapping algorithm. For each linear distance the null hypothesis is rejected if the 90% confidence interval does not include 1

(FDM) or 0 (SDM): Rejection of the null hypothesis enables localization of differences to specific landmarks and linear distances.

Bootstrap Distribution of T (FDM) or Z (SDM) was calculated as follow: For each FDM is calculated a T value. The location of the T observed from the FDM, allows calculate the probability (*P*) in this distribution.

Stereological procedures

Five WT, five CD mice were perfused transcardially with fixative (4% paraformaldehyde). Brains were removed and placed in fixative. Brains were processed for stereology according to the procedure detailed in Supplemental Methods. Briefly, brains embedded in glycolmethacrylate (Tecnovit 7100; Heraeus Kulzer, Werheim, Germany) were cut and then collected on a noncoated glass slide, stained with Giemsa, and mounted with Entellan New (Merck, Darmstadt, Germany). Volume and neuronal number estimations were performed using StereoInvestigator software (Microbrightfield, Williston, VT) and a camera (DXC-390; Sony, Tokyo, Japan) attached to a motorized microscope Visiopharm Integrator System, Olympus BX51. Cavalieri's principle (61) was used to assess the volume of each region.

Immunohistochemistry

12 weeks old mice were transcardially perfused with 4% paraformaldehyde in 0.1 M phosphate buffer. Brains were removed and postfixed in the same buffer for 24 h at 4°C. Thereafter, they were cryoprotected in 30% sucrose, frozen on dry ice, and sectioned on a cryostat. Serial coronal or sagittal (40 µm-thick) sections were collected in a cryoprotectant solution (30% glycerol, 30% ethylene glycol, 40% 0.1 M phosphate buffer [pH 7.4]). For Doublecortin immunohistochemistry was performed using the ImmunoCruz goat ABC Staining System, Santa Cruz Biotechnology INC (Santa Cruz, USA) following the manufacturer's instructions. Briefly, endogenous peroxidase was blocked with 3% H_2O_2 solution and washed with a solution of 0.2% Triton X-100 in PBS. Sections were blocked (1.5% blocking serum in PBS) and incubated overnight at 4°C with a goat polyclonal

antibody against Doublecortin (Santa Cruz Biotechnology, INC) diluted (1:300) in 1.5% blocking solution. Sections were incubated with a biotinylated secondary antibody following manufacturer's instructions, Positive signals were developed with a diaminobenzidine substrate by using the avidin-biotin-peroxidase system according to the manufacturer's instructions.

For GFAP immunofluorescence, sections were blocked (1.5% blocking serum in PBS) and incubated overnight at 4°C with a mouse monoclonal antibody against GFAP (MAB360, Millipore, 1:500). Sections were incubated with an Alexa Fluor 555 conjugated secondary antibody (Invitrogen 1:1000).

Imaging

1024x1024 pixel confocal fluorescence image stacks were obtained using a HC PL FLUOTAR 20x 0.5 DRY objective in a TCS SP2 LEICA microscope. Multichannel imaging was done sequentially. Neuronal density was measured by staining 200µm coronal tissue sections with the neuron-specific fluorescent Nissl stain Neurotrace 530/615 (Invitrigen 1:250). Only superficial ($\leq$ 40 µm depth) tissue was imaged due to limited dye penetration. Counts from five tissue sections per animal (3-5 mice) were averaged for each brain region analyzed.

For qualitative analysis of YFP expression patterns, and for P12-14 YFP$^+$ cell counting, 1249x956 pixel wide-field images of cerebral hemispheres were obtained using a 1.6X projection lens on a Leika epifluorescence microscope. Images were captured with a CCD camera (Leika). We used ImageJ sofware for all the image analysis. More detailed methodology for dendritic length measures and spine density calculi can be found in Supplemental Methods.

Behavior testing

Behavior testing was performed in the Parc de Recerca Biomèdica de Barcelona (PRBB) mouse facility using males, 15 WT and 15 CD. Testing was performed from the least to the most aversive test (see expand protocols in Supplemental Methods).

The Shirpa protocol was performed as previously described (62). The rotarod test to evaluate motor coordination and balance was assessed with a commercially available rotarod apparatus (Rotarod LE8500. Panlab, Harvard Apparatus, Spain).

Animals were tested in a visuo-spatial learning acquisition paradigm in the Water Maze test (WM). Escape latencies, length of the swimming paths and swimming speed for each animal and trial were monitored and computed by a software tracking system SMART© (Panlab, Harvard Apparatus, Spain) connected to a video camera placed above the pool.

Pure contextual fear conditioning paradigm was performed by pairing an initially neutral context (CS, conditioned stimulus) with an aversive stimulus such as an electric foot shock (US, unconditioned stimulus) to elicit a freezing response, a reliable measure of conditioned fear in rodents.

The acoustic startle response was measured with Panlab startle response apparatus (Panlab, Harvard Apparatus Spain). The mice were given 15 min habituation to the apparatus and then exposed to a single 120 dB pulse in a single session. The startle response was recorded for 65 ms.

For the treadmill (Panlab, Harvard Apparatus Spain) mice were placed on the top of the already moving belt facing away from the electrified grid and in the direction opposite to the movement of the belt. Thus, to avoid the foot shocks, the mice had to move forward. Whenever an animal fell off the belt, foot shocks were applied for a maximal duration of 1 s and with an interval of 2 s between every shock. After the shocks, mice were retrieved and placed back on the still moving belt to facilitate the association between safety and the belt.

For social behavior mice were presented with a novel mouse in a wire cup-like container large enough to hold a single mouse (7 cm diameter x 10 cm high), adapted from a social approach/interaction test previously described (46). The test was conducted in an open field (50 x 50 cm) with illumination (50 lux). Test subjects were placed in the center compartment and allowed a 10-minute habituation period. In the trials an unfamiliar mouse (same strain) was introduced in the wire cup-like container. The amount of time spent investigating the novel mouse was scored in three 5-minute segments followed by an additional 5-minute segment with a second novel mouse. After one 3 minutes inter trial interval in which the entire setup was thoroughly cleaned to eliminate olfactory cues a second novel unfamiliar mouse was introduced in the wire cup-like container. Subject activity was scored manually (by at least two investigators) as the time that the subject was in nose-to-cage investigation of the novel stimulus in a 5-minutes segment. In all experiments investigators were blinded to genotypes.

Statistical analyses

All data are presented as means ± SEM. Media comparisons between groups were performed using t-test for paired value or U de Mann-Whitney as non-parametric test. A General Linear Models of repeated measures ANOVA was used in some test. All statistical tests were made under the SPSS environment. Values of $P<0.05$ were considered significant.

ACKNOWLEDGEMENTS

The authors gratefully acknowledge Verena Terrado for technical assistance, Thais Freitas for her help in the brain doublecortin analysis, Miren Bravo for her help in the YFP$^+$ cells counting, Gabriela Palacios for statistical assistance and Dr.Isidro García-Sánchez for providing the cre-loxP vectors. This work was supported by the Spanish Ministry of Ecomomy and Competitivity to V.C. (grant SAF2012-40036), the European AnEuploidy project to L.P.J., M.D. and Y.H. The Rare Diseases CIBER (CIBERER) Fellowship supported M.S-P. and C.B.

CONFLICT OF INTEREST STATEMENT

None declared

REFERENCES

1. P. Stromme, P. G. Bjornstad and K. Ramstad. (2002) Prevalence estimation of Williams syndrome. *J. Child. Neurol.,* **17**, 269-271.

2. A. L. Perez Jurado. (2003) Williams-Beuren syndrome: a model of recurrent genomic mutation. *Horm. Res.,* **59 Suppl 1**, 106-113.

3. C. Schubert. (2009) The genomic basis of the Williams-Beuren syndrome. *Cell. Mol. Life Sci.,* **66**, 1178-1197.

4. M. Bayes, L. F. Magano, N. Rivera, R. Flores and L. A. Perez Jurado. (2003) Mutational mechanisms of Williams-Beuren syndrome deletions. *Am. J. Hum. Genet.,* **73**, 131-151.

5. R. Peoples, Y. Franke, Y. K. Wang, L. Perez-Jurado, T. Paperna, M. Cisco and U. Francke. (2000) A physical map, including a BAC/PAC clone contig, of the Williams-Beuren syndrome--deletion region at 7q11.23. *Am. J. Hum. Genet.,* **66**, 47-68.

6. B. R. Pober. (2010) Williams-Beuren syndrome. *N. Engl. J. Med.,* **362**, 239-252.

7. A. Wessel, R. Motz, R. Pankau and J. H. Bursch. (1997) [Arterial hypertension and blood pressure profile in patients with Williams-Beuren syndrome]. *Z. Kardiol.,* **86**, 251-257.

8. C. V. Dilts, C. A. Morris and C. O. Leonard. (1990) Hypothesis for development of a behavioral phenotype in Williams syndrome. *Am. J. Med. Genet. Suppl,* **6**, 126-131.

9. C. Gagliardi, S. Martelli, M. D. Burt and R. Borgatti. (2007) Evolution of neurologic features in Williams syndrome. *Pediatr. Neurol.,* **36**, 301-306.

10. M. A. Martens, S. J. Wilson and D. C. Reutens. (2008) Research Review: Williams syndrome: a critical review of the cognitive, behavioral, and neuroanatomical phenotype. *J. Child. Psychol. Psychiatry,* **49**, 576-608.

11. C. B. Mervis, B. F. Robinson, J. Bertrand, C. A. Morris, B. P. Klein-Tasman and S. C. Armstrong. (2000) The Williams syndrome cognitive profile. *Brain Cogn.,* **44**, 604-628.

12. A. P. Jackowski, K. Rando, C. Maria de Araujo, C. G. Del Cole, I. Silva and A. L. Tavares de Lacerda. (2009) Brain abnormalities in Williams syndrome: a review of structural and functional magnetic resonance imaging findings. *Eur J Paediatr. Neurol.,* **13**, 305-316.

13. A. Meyer-Lindenberg, C. B. Mervis, D. Sarpal, P. Koch, S. Steele, P. Kohn, S. Marenco, C. A. Morris, S. Das, S. Kippenhan, et al. (2005) Functional, structural, and metabolic abnormalities of the hippocampal formation in Williams syndrome. *J. Clin. Invest.,* **115**, 1888-1895.

14. M. Del Campo, A. Antonell, L. F. Magano, F. J. Munoz, R. Flores, M. Bayes and L. A. Perez Jurado. (2006) Hemizygosity at the NCF1 gene in patients with Williams-Beuren syndrome decreases their risk of hypertension. *Am. J. Hum. Genet.,* **78**, 533-542.

15. K. Metcalfe, A. K. Rucka, L. Smoot, G. Hofstadler, G. Tuzler, P. McKeown, V. Siu, A. Rauch, J. Dean, N. Dennis, et al. (2000) Elastin: mutational spectrum in supravalvular aortic stenosis. *Eur. J. Hum. Genet.,* **8**, 955-963.

16. V. Campuzano, M. Segura-Puimedon, V. Terrado, C. Sanchez-Rodriguez, M. Coustets, M. Menacho-Marquez, J. Nevado, X. R. Bustelo, U. Francke and L. A. Perez-Jurado. (2012) Reduction of NADPH-oxidase activity ameliorates the cardiovascular phenotype in a mouse model of Williams-Beuren Syndrome. *PLoS Genet.,* **8**, e1002458.

17. T. F. Doyle, U. Bellugi, J. R. Korenberg and J. Graham. (2004) "Everybody in the world is my friend" hypersociability in young children with Williams syndrome. *Am. J. Med. Genet. A,* **124A**, 263-273.

18. M. Tassabehji, P. Hammond, A. Karmiloff-Smith, P. Thompson, S. S. Thorgeirsson, M. E. Durkin, N. C. Popescu, T. Hutton, K. Metcalfe, A. Rucka, et al. (2005) GTF2IRD1 in craniofacial development of humans and mice. *Science,* **310**, 1184-1187.

19. U. DeSilva, H. Massa, B. J. Trask and E. D. Green. (1999) Comparative mapping of the region of human chromosome 7 deleted in williams syndrome. *Genome Res.,* **9**, 428-436.

20. M. C. Valero, O. de Luis, J. Cruces and L. A. Perez Jurado. (2000) Fine-scale comparative mapping of the human 7q11.23 region and the orthologous region on mouse chromosome 5G: the low-copy repeats that flank the Williams-Beuren syndrome deletion arose at breakpoint sites of an evolutionary inversion(s). *Genomics,* **69**, 1-13.

21. S. Capossela, L. Muzio, A. Bertolo, V. Bianchi, G. Dati, L. Chaabane, C. Godi, L. S. Politi, S. Biffo, P. D'Adamo, et al. (2012) Growth defects and impaired cognitive-behavioral abilities in mice with knockout for Eif4h, a gene located in the mouse homolog of the Williams-Beuren syndrome critical region. *Am. J. Pathol.,* **180**, 1121-1135.

22. C. C. Hoogenraad, B. Koekkoek, A. Akhmanova, H. Krugers, B. Dortland, M. Miedema, A. van Alphen, W. M. Kistler, M. Jaegle, M. Koutsourakis, et al. (2002) Targeted mutation of Cyln2 in the Williams syndrome critical region links CLIP-115 haploinsufficiency to neurodevelopmental abnormalities in mice. *Nat. Genet.,* **32**, 116-127.

23. D. Y. Li, B. Brooke, E. C. Davis, R. P. Mecham, L. K. Sorensen, B. B. Boak, E. Eichwald and M. T. Keating. (1998) Elastin is an essential determinant of arterial morphogenesis. *Nature,* **393**, 276-280.

24. J. Lucena, S. Pezzi, E. Aso, M. C. Valero, C. Carreiro, P. Dubus, A. Sampaio, M. Segura, I. Barthelemy, M. Y. Zindel, et al. (2010) Essential role of the N-terminal region of TFII-I in viability and behavior. *BMC Med. Genet.,* **11**, 61.

25. K. Yoshimura, H. Kitagawa, R. Fujiki, M. Tanabe, S. Takezawa, I. Takada, I. Yamaoka, M. Yonezawa, T. Kondo, Y. Furutani, et al. (2009) Distinct function of 2 chromatin remodeling complexes that share a common subunit, Williams syndrome transcription factor (WSTF). *Proc. Natl. Acad. Sci. U S A,* **106**, 9280-9285.

26. H. H. Li, M. Roy, U. Kuscuoglu, C. M. Spencer, B. Halm, K. C. Harrison, J. H. Bayle, A. Splendore, F. Ding, L. A. Meltzer, et al. (2009) Induced chromosome deletions cause hypersociability and other features of Williams-Beuren syndrome in mice. *EMBO Mol. Med.,* **1**, 50-65.

27. B. Enkhmandakh, A. V. Makeyev, L. Erdenechimeg, F. H. Ruddle, N. O. Chimge, M. I. Tussie-Luna, A. L. Roy and D. Bayarsaihan. (2009) Essential functions of the Williams-Beuren syndrome-associated TFII-I genes in embryonic development. *Proc. Natl. Acad. Sci. U S A,* **106**, 181-186.

28. C. A. Morris, S. A. Demsey, C. O. Leonard, C. Dilts and B. L. Blackburn. (1988) Natural history of Williams syndrome: physical characteristics. *J. Pediatr.,* **113**, 318-326.

29. R. C. Ignacio, Jr., W. P. Klapheke, T. Stephen and S. Bond. (2012) Diverticulitis in a child with Williams syndrome: a case report and review of the literature. *J. Pediatr. Surg.,* **47**, E33-35.

30. C. J. Goergen, H. H. Li, U. Francke and C. A. Taylor. (2011) Induced chromosome deletion in a Williams-Beuren syndrome mouse model causes cardiovascular abnormalities. *J. Vasc. Res.,* **48**, 119-129.

31. P. Hammond, T. J. Hutton, J. E. Allanson, B. Buxton, L. E. Campbell, J. Clayton-Smith, D. Donnai, A. Karmiloff-Smith, K. Metcalfe, K. C. Murphy, et al. (2005) Discriminating power of localized three-dimensional facial morphology. *Am. J. Hum. Genet.,* **77**, 999-1010.

32. A. Ashe, D. K. Morgan, N. C. Whitelaw, T. J. Bruxner, N. K. Vickaryous, L. L. Cox, N. C. Butterfield, C. Wicking, M. E. Blewitt, S. J. Wilkins, et al. (2008) A genome-wide screen for modifiers of transgene variegation identifies genes with critical roles in development. *Genome Biol.,* **9**, R182.

33. L. E. Campbell, E. Daly, F. Toal, A. Stevens, R. Azuma, A. Karmiloff-Smith, D. G. Murphy and K. C. Murphy. (2009) Brain structural differences associated with the behavioural phenotype in children with Williams syndrome. *Brain Res.,* **1258**, 96-107.

34. M. C. Chiang, A. L. Reiss, A. D. Lee, U. Bellugi, A. M. Galaburda, J. R. Korenberg, D. L. Mills, A. W. Toga and P. M. Thompson. (2007) 3D pattern of brain abnormalities in Williams syndrome visualized using tensor-based morphometry. *Neuroimage,* **36**, 1096-1109.

35. S. A. Meda, J. R. Pryweller and T. A. Thornton-Wells. (2012) Regional brain differences in cortical thickness, surface area and subcortical volume in individuals with Williams syndrome. *PLoS One,* **7**, e31913.

36. A. L. Reiss, M. A. Eckert, F. E. Rose, A. Karchemskiy, S. Kesler, M. Chang, M. F. Reynolds, H. Kwon and A. Galaburda. (2004) An experiment of nature: brain anatomy parallels cognition and behavior in Williams syndrome. *J. Neurosci.,* **24**, 5009-5015.

37. A. L. Reiss, S. Eliez, J. E. Schmitt, E. Straus, Z. Lai, W. Jones and U. Bellugi. (2000) IV. Neuroanatomy of Williams syndrome: a high-resolution MRI study. *J. Cogn. Neurosci.,* **12 Suppl 1**, 65-73.

38. J. E. Schmitt, S. Eliez, I. S. Warsofsky, U. Bellugi and A. L. Reiss. (2001) Corpus callosum morphology of Williams syndrome: relation to genetics and behavior. *Dev. Med. Child. Neurol.,* **43**, 155-159.

39. F. Tomaiuolo, M. Di Paola, B. Caravale, S. Vicari, M. Petrides and C. Caltagirone. (2002) Morphology and morphometry of the corpus callosum in Williams syndrome: a T1-weighted MRI study. *Neuroreport,* **13**, 2281-2284.

40. A. M. Galaburda, D. P. Holinger, U. Bellugi and G. F. Sherman. (2002) Williams syndrome: neuronal size and neuronal-packing density in primary visual cortex. *Arch. Neurol.,* **59**, 1461-1467.

41. J. A. Marler, J. L. Elfenbein, B. M. Ryals, Z. Urban and M. L. Netzloff. (2005) Sensorineural hearing loss in children and adults with Williams syndrome. *Am. J. Med. Genet. A,* **138**, 318-327.

42. C. B. Mervis and A. M. Becerra. (2007) Language and communicative development in Williams syndrome. *Ment. Retard. Dev. Disabil. Res. Rev.,* **13**, 3-15.

43. T. Schneider, Z. Skitt, Y. Liu, R. M. Deacon, J. Flint, A. Karmiloff-Smith, J. N. Rawlins and M. Tassabehji. (2012) Anxious, hypoactive phenotype combined with motor deficits in Gtf2ird1 null mouse model relevant to Williams syndrome. *Behav. Brain Res.,* **233**, 458-473.

44. H. C. Pape and O. Stork. (2003) Genes and mechanisms in the amygdala involved in the formation of fear memory. *Ann. N. Y. Acad. Sci.,* **985**, 92-105.

45. A. Jarvinen-Pasley, U. Bellugi, J. Reilly, D. L. Mills, A. Galaburda, A. L. Reiss and J. R. Korenberg. (2008) Defining the social phenotype in Williams syndrome: a model for linking gene, the brain, and behavior. *Dev. Psychopathol.,* **20**, 1-35.

46. T. Sakurai, N. P. Dorr, N. Takahashi, L. A. McInnes, G. A. Elder and J. D. Buxbaum. (2011) Haploinsufficiency of Gtf2i, a gene deleted in Williams Syndrome, leads to increases in social interactions. *Autism Res.,* **4**, 28-39.

47. C. A. Morris and C. B. Mervis. (2000) Williams syndrome and related disorders. *Annu. Rev. Genomics Hum. Genet.,* **1**, 461-484.

48. B. N. Blackwell, T. J. Bucci, R. W. Hart and A. Turturro. (1995) Longevity, body weight, and neoplasia in ad libitum-fed and diet-restricted C57BL6 mice fed NIH-31 open formula diet. *Toxicol. Pathol.,* **23**, 570-582.

49. B. R. Pober, M. Johnson and Z. Urban. (2008) Mechanisms and treatment of cardiovascular disease in Williams-Beuren syndrome. *J. Clin. Invest.,* **118**, 1606-1615.

50. K. Broder, E. Reinhardt, J. Ahern, R. Lifton, W. Tamborlane and B. Pober. (1999) Elevated ambulatory blood pressure in 20 subjects with Williams syndrome. *Am. J. Med. Genet.,* **83**, 356-360.
51. S. Axelsson, I. Kjaer, A. Heiberg, T. Bjornland and K. Storhaug. (2005) Neurocranial morphology and growth in Williams syndrome. *Eur. J. Orthod.,* **27**, 32-47.
52. E. Mass and L. Belostoky. (1993) Craniofacial morphology of children with Williams syndrome. *Cleft Palate Craniofac. J.,* **30**, 343-349.
53. D. R. Hocking, J. L. Bradshaw and N. J. Rinehart. (2008) Fronto-parietal and cerebellar contributions to motor dysfunction in Williams syndrome: a review and future directions. *Neurosci. Biobehav. Rev.,* **32**, 497-507.
54. L. Capitao, A. Sampaio, C. Sampaio, C. Vasconcelos, M. Fernandez, E. Garayzabal, M. E. Shenton and O. F. Goncalves. (2011) MRI amygdala volume in Williams Syndrome. *Res. Dev. Disabil.,* **32**, 2767-2772.
55. D. P. Stuss, J. D. Boyd, D. B. Levin and K. R. Delaney. (2012) MeCP2 mutation results in compartment-specific reductions in dendritic branching and spine density in layer 5 motor cortical neurons of YFP-H mice. *PLoS One,* **7**, e31896.
56. A. E. Power and J. L. McGaugh. (2002) Cholinergic activation of the basolateral amygdala regulates unlearned freezing behavior in rats. *Behav. Brain Res.,* **134**, 307-315.
57. G. Feng, R. H. Mellor, M. Bernstein, C. Keller-Peck, Q. T. Nguyen, M. Wallace, J. M. Nerbonne, J. W. Lichtman and J. R. Sanes. (2000) Imaging neuronal subsets in transgenic mice expressing multiple spectral variants of GFP. *Neuron,* **28**, 41-51.
58. G. J. Todaro and H. Green. (1967) Simian virus 40 transformation and the period of cellular deoxyribonucleic acid synthesis. *J. Virol.,* **1**, 115-119.
59. C. Pantoja and M. Serrano. (1999) Murine fibroblasts lacking p21 undergo senescence and are resistant to transformation by oncogenic Ras. *Oncogene,* **18**, 4974-4982.
60. S. Rozen and H. Skaletsky. (2000) Primer3 on the WWW for general users and for biologist programmers. *Methods Mol. Biol.,* **132**, 365-386.
61. H. J. Gundersen, T. F. Bendtsen, L. Korbo, N. Marcussen, A. Moller, K. Nielsen, J. R. Nyengaard, B. Pakkenberg, F. B. Sorensen, A. Vesterby, et al. (1988) Some new, simple and efficient stereological methods and their use in pathological research and diagnosis. *APMIS,* **96**, 379-394.
62. D. C. Rogers, E. M. Fisher, S. D. Brown, J. Peters, A. J. Hunter and J. E. Martin. (1997) Behavioral and functional analysis of mouse phenotype: SHIRPA, a proposed protocol for comprehensive phenotype assessment. *Mamm. Genome,* **8**, 711-713.

LEGENDS TO FIGURES

Figure 1. Generation and characterization of a CD cell line (ESSP9) and mice

(A) Schematic diagram of the WBSCR in mouse chromosome band 5G2 and the targeting strategy used. ESSP9 represents the recombined chromosome with the complete deletion in the ES cell line that was finally used to generate the genetically modified CD mice. **(B)** Left, representative FISH picture showing "*in cis*" integration of 2LoxP sites (green dots, HPRT probe). Right, MLPA analysis of ESSP9 DNA with a custom-made panel. The normalized peak ratios were 1 for the two external genes of the same chromosome (*Cutl-1* and *Wbscr17)* and 0.5 for the genes in the deletion (*Gtf2i, Limk1, Cyln2, Fkbp6*, *Baz1b* and *Rcf2*) indicating the heterozygous copy loss. **(C)** Relative gene transcript levels of seven deleted genes in five different tissues of CD mice by RT-PCR. Data were normalized so the mean of the WT group was 1. Analyses were performed in triplicate. Samples were pools of three animals. The results represent the mean ± SEM

Figure 2. Craniofacial analyses in CD females

(A) The cranial analysis showed no global differences in the size of the skull of the CD females, although a tendency to smaller nose was observed (*P*=0.122). **(B)** Representative reconstructed 3D skull images showing the most interesting ratios altered in CD mice. **(C)** A reduced size of the mandible was evident in the CD mice when compared to the WT (*P* =0.028). **(D)** Representative reconstructed 3D mandible images of CD mice showing smaller size shifting distances. Pointed, features with points below mandible. Red lines, smaller distance (ratio<0.960); Green lines, smaller distance (0.960<ratio<1). N=15 females per group.

Figure 3. Neurological analysis of CD and WT animals.

(A) Comparison of brain weights of CD and WT adult mice (16-21 weeks old). N=13-14 genotype for males; N=13-14 genotype for females. **(B)** Cellular density in different areas of the amygdala showing significant reduction in CD mice in Basolateral area. LA, lateral amygdala; BLA, basolateral amygdala; CeA, central amygdala; TA, total amygdala. N=5 mice/group. **(C)** Bar graph represents the average volumes of CA3 regions for 5 mice per group. SO, stratus oriens; SP, stratus pyramidalis; SR, stratus radiatus. **(D)** Neural density in the cellular layer of dentate gyrus after doublecortin (Dcx) staining. Data are presented as means ± SEM. *P* values are shown with asterisks indicating values that are significantly different in individual group comparisons (U Mann-Whitney test). *, $P< 0.05$); **, $P\leq 0.01$; ***, $P \leq 0.001$. Blue squares: WT males; Red squares: CD males.

Figure 4. CD mutant males have reduced numbers of YFP-expressing pyramidal neurons. **(A)** Fewer YFP^+ cells are observed across the entire cortex and hippocampus in mutant males (150 µm coronal sections, ≈ Bregma 0.74 and -1.28 mm in WT). Some regions are more dramatically affected than others, such as the somatosensory cortex (red arrow), motor cortex (blue arrow) and CA1 region (green arrow). Sharp boundaries correspond to functional regions (SS, somatosensory; M, motor). **(B)** Fluorescent Nissl staining (red) of the L5 somatosensory and motor cortex and pyramidal neurons of the CA1 region. A limited subset of pyramidal neurons expresses YFP. Scale bar = 100µm. **(C)** The percentage of YFP^+ pyramidal neurons was reduced in motor (M), somatosensory (SS) and cortical regions as well as YFP^+ density in CA1 hippocampal region. **(D)** The number of YFP^+ pyramidal cells was significantly reduced as early as P12-P14 developmental stage in cortex ($P= 0.036$) and almost in hippocampus ($P=0.057$) N=3 WT and 5 CD males. Data are presented as means ± SEM. *P* values are shown with asterisks indicating values that are significantly different in individual group comparisons (U Mann-Whitney test). *, $P< 0.05$); ***, $P \leq 0.001$. Blue squares: WT males; Red squares: CD males.

Figure 5. CD mice have deficits in motor function and abnormal response to noise.

(A) A significant deficit (0=Normal; 8=Deficit) in Motricity Tonus Strength, measured as a compound of wire maneuver and hindlimb tone, was present in CD males (*P*=0.002). **(B)** The rotarod test to evaluate motor coordination and balance was assessed. A significant deficiency is observed as soon as 7 r.p.m. (*P*=0.043) and continuing through 10 r.p.m. (*P*=0.007), 14 r.p.m. (*P*<0.001), 19 r.p.m. (*P*<0.001), until 24 r.p.m (*P*=0.001). **(C)** Complete deletion mice have abnormal startle response to PPI (*P* =0.025). Responses to 120 dB white noise sound were recorded (acoustic startle response). Results represent the mean ± SEM in all cases (N=12-8 per group). *P* values are shown with asterisks indicating values that are significantly different in individual group comparisons (U Mann-Whitney test).*, P<0.05; **, P<0.01. Blue squares or lines: WT males; Red squares or lines: CD males.

Figure 6. Water Maze test results in CD mice.

(A) Significant differences were found in distance in pre-training (*P*=0.045), or in the acquisition sessions (A2: *P*=0.011; A3: *P*=0.021). **(B)** Regarding the average speed significant differences were found in almost all sessions (re-training, *P*=0.064; A3: *P*=0.004; A4: *P*=0.021; A5: *P*=0.045; A6: *P*=0.031). **(C)** In WM, in the probe session (Removal) CD mice spent more time across the trained quadrant (NE) than WT mice (*P*=0.069) and significantly less (*P*=0.047) in the adjacent quadrant (NW). **(D)** When Reversal session was analyzed, where cognitive flexibility is evaluated, a significant reduction in swimming speed was shown in CD mice in reversal session 1 (*P*=0.025) and in reversal session 2 (*P*=0.037). Results represent the mean ± SEM in all cases (N=12-8 per group). *P* values are shown with asterisks indicating values that are significantly different in individual group comparisons (U Mann-Whitney test).*, *P*<0.05; **, *P*<0.01. Blue squares or lines: WT males; Red squares or lines: CD males.

Figure 7. Social behavior

(A) WT or CD mice were allowed to explore an unfamiliar mouse in a wire cup-like container placed in an open field. Time spent exploring the novel mouse was scored in two 5-minute segments (0–5, S1 and 5–10. S2). We observed that WT mice exhibited an habituation effect, exploring the novel mouse for less time during the second 5-minute segment than during the first (*P*=0.007). **(B)** Significant differences between genotypes are observed in the time spent in nose-to-cage contact by cage approach in the first (RS1, *P*=0.003) and third (RS3, *P*=0.004) segments. **(C)** Total exploration time is significantly higher in CD respect to WT littermates (*P*=0.001). **(D)** A repeated measures ANOVA showed a significant difference of time-genotype. ($F_{1,17}$=19,563, $P \leq 0.001$). Results represent the mean ± SEM in all cases (N=12-8 per group). *P* values are shown with asterisks indicating values that are significantly different in individual group comparisons (U Mann-Whitney test).**, $P \leq 0.01$; ***, $P \leq 0.001$. Blue squares or lines: WT males; Red squares or lines: CD males.

Table 1: Cardiovascular parameters of CD and WT mice

Parameter	WT	CD
Mean BP (mm Hg)	84.2 ±7.88	112.85 ± 6.13*
Heart rate (bpm)	630 ± 37.44	569.4 ± 81.51
Body weight (g)	42.19 ± 3.24	38.74 ± 2.91
Heart weight (g)	0.196 ± 0.0075	0.184 ± 0.0097
Heart weight/ Body weight	0.45 ± 0.013	0.55 ± 0.021***
Aorta wall thickness (μm)	62.87 ± 2.30	69.64 ± 3.26
Lamellar units in aorta	7.17 ± 0.48	7.83 ± 0.48

P values are shown with asterisks indicating values that are significantly different in individual group comparisons (U Mann-Whitney test).*, *P*≤0.05; ***, *P*≤0.001

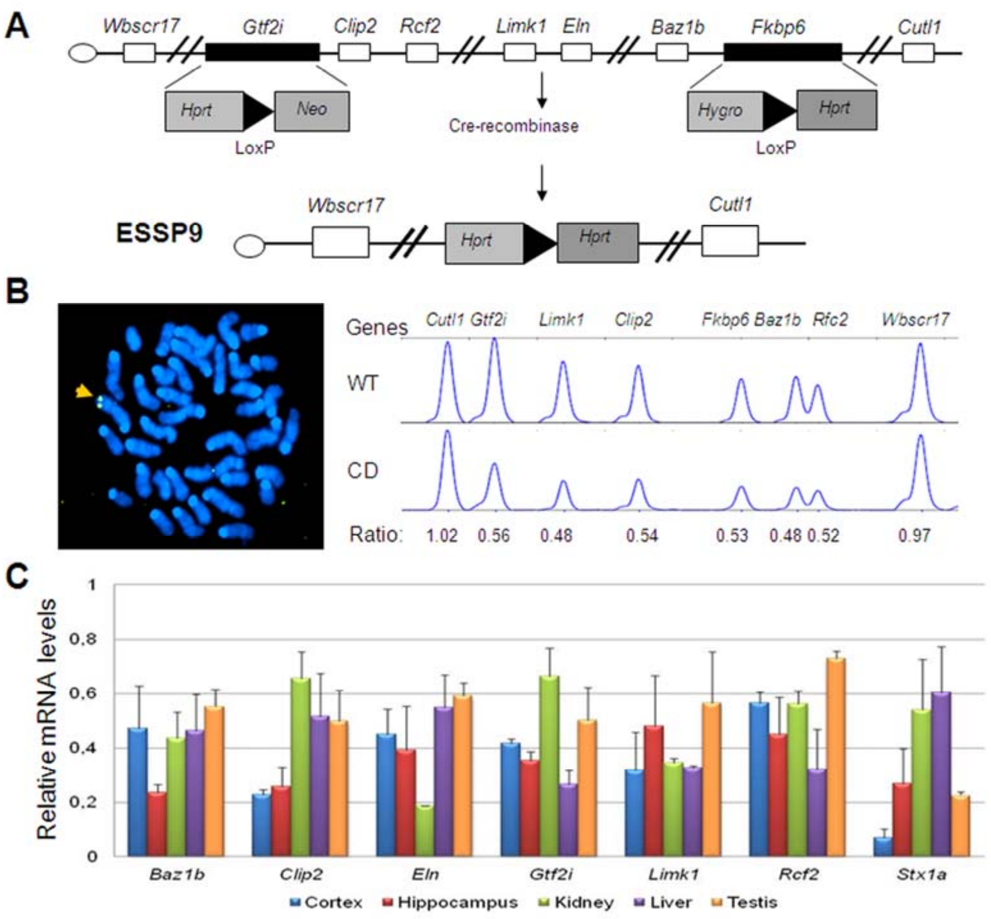
A
Wbscr17
Gtf2i
Clip2
Rcf2
Limk1
Eln
Baz1b
Fkbp6
Cutl1
Hprt
Neo
LoxP
Cre-recombinase
Hygro
Hprt
LoxP
ESSP9
Wbscr17
Hprt
Hprt
Cutl1
B
Genes
Cutl1
Gtf2i
Limk1
Clip2
Fkbp6
Baz1b
Rfc2
Wbscr17
WT
CD
Ratio:
1.02
0.56
0.48
0.54
0.53
0.48
0.52
0.97
C
Relative mRNA levels
1
0,8
0,6
0,4
0,2
0
Baz1b
Clip2
Eln
Gtf2i
Limk1
Rcf2
Stx1a
Cortex
Hippocampus
Kidney
Liver
Testis

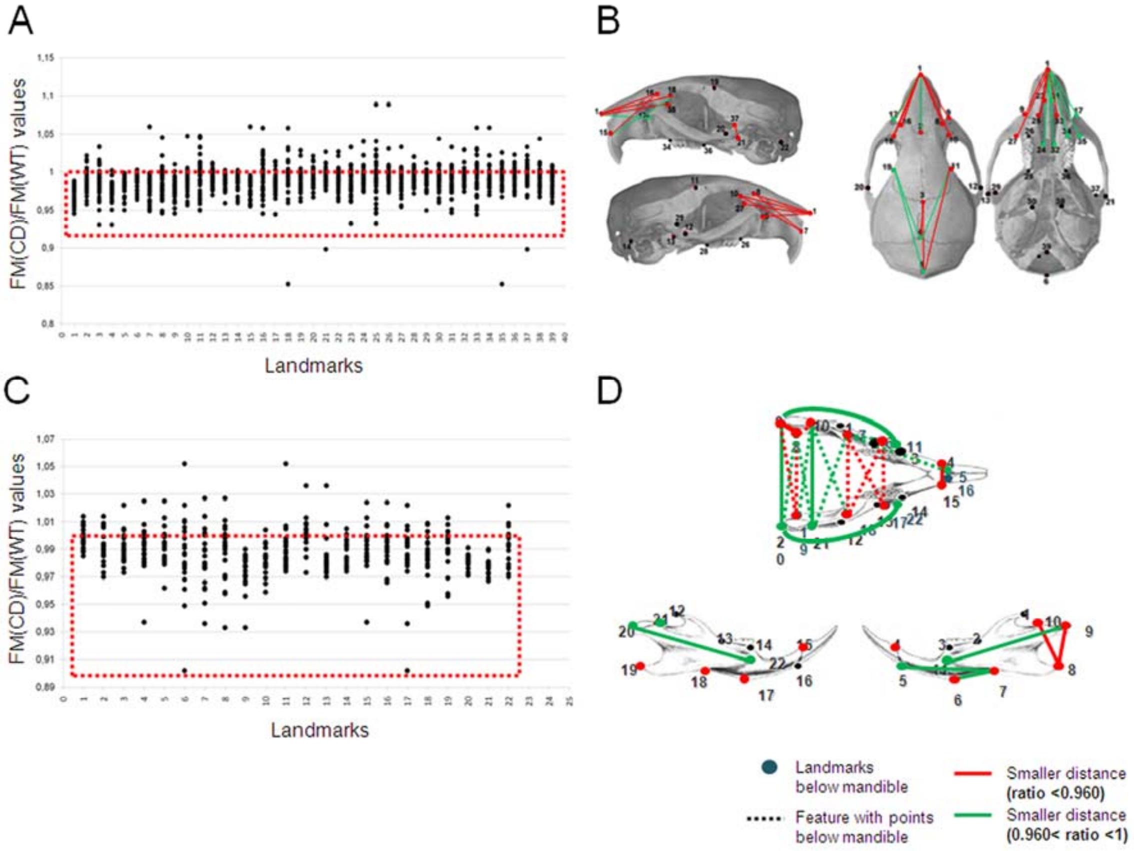
A
B
C
D
FM(CD)/FM(WT) values
Landmarks
FM(CD)/FM(WT) values
Landmarks
Landmarks below mandible
Feature with points below mandible
Smaller distance (ratio <0.960)
Smaller distance (0.960< ratio <1)

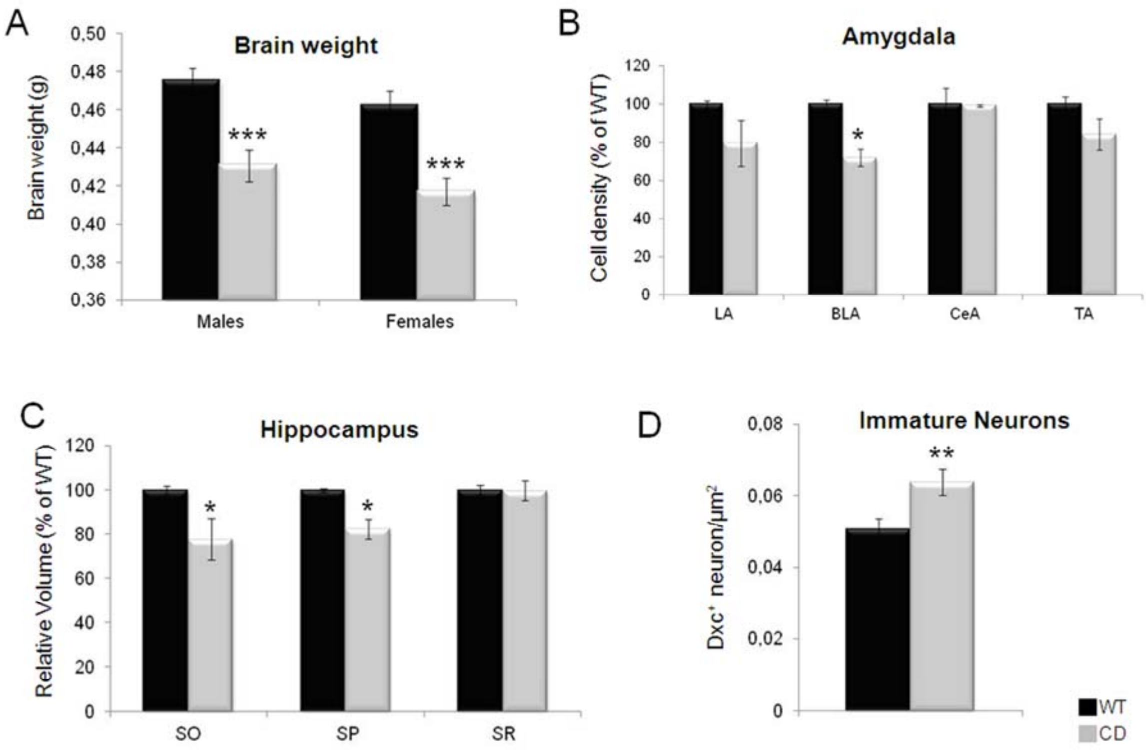
A
Brain weight
Brain weight (g)
0,50
0,48
0,46
0,44
0,42
0,40
0,38
0,36
***
***
Males
Females
B
Amygdala
Cell density (% of WT)
120
100
80
60
40
20
0
*
LA
BLA
CeA
TA
C
Hippocampus
Relative Volume (% of WT)
120
100
80
60
40
20
0
*
*
SO
SP
SR
D
Immature Neurons
Dxc+ neuron/µm2
0,08
0,06
0,04
0,02
0
**
WT
CD

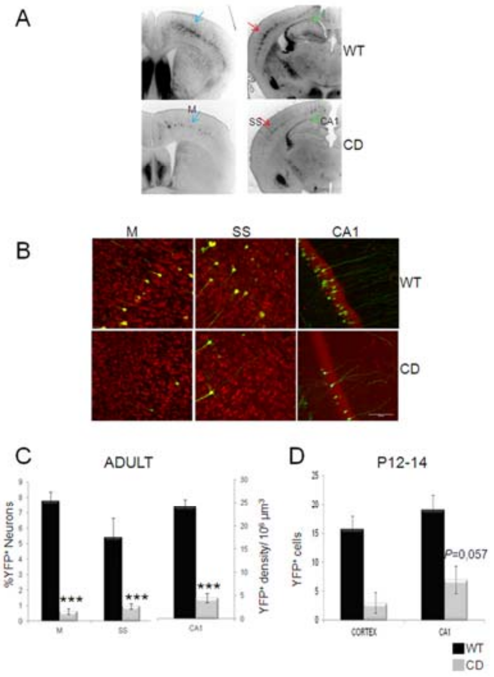
A
M
SS
CA1
WT
CD
B
M
SS
CA1
WT
CD
C
ADULT
%YFP⁺ Neurons
YFP⁺ density/ 10⁶ µm³
0
1
2
3
4
5
6
7
8
9
0
5
10
15
20
25
30
***
***
***
M
SS
CA1
D
P12-14
YFP⁺ cells
0
5
10
15
20
25
P=0,057
CORTEX
CA1
WT
CD

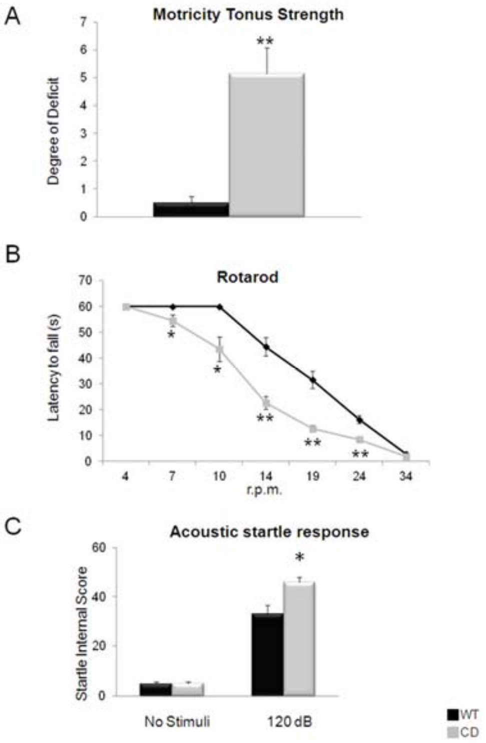
A
Motricity Tonus Strength
Degree of Deficit
0
1
2
3
4
5
6
7
**
B
Rotarod
Latency to fall (s)
0
10
20
30
40
50
60
70
4
7
10
14
19
24
34
r.p.m.
*
*
**
**
**
C
Acoustic startle response
Startle Internal Score
0
20
40
60
*
No Stimuli
120 dB
WT
CD

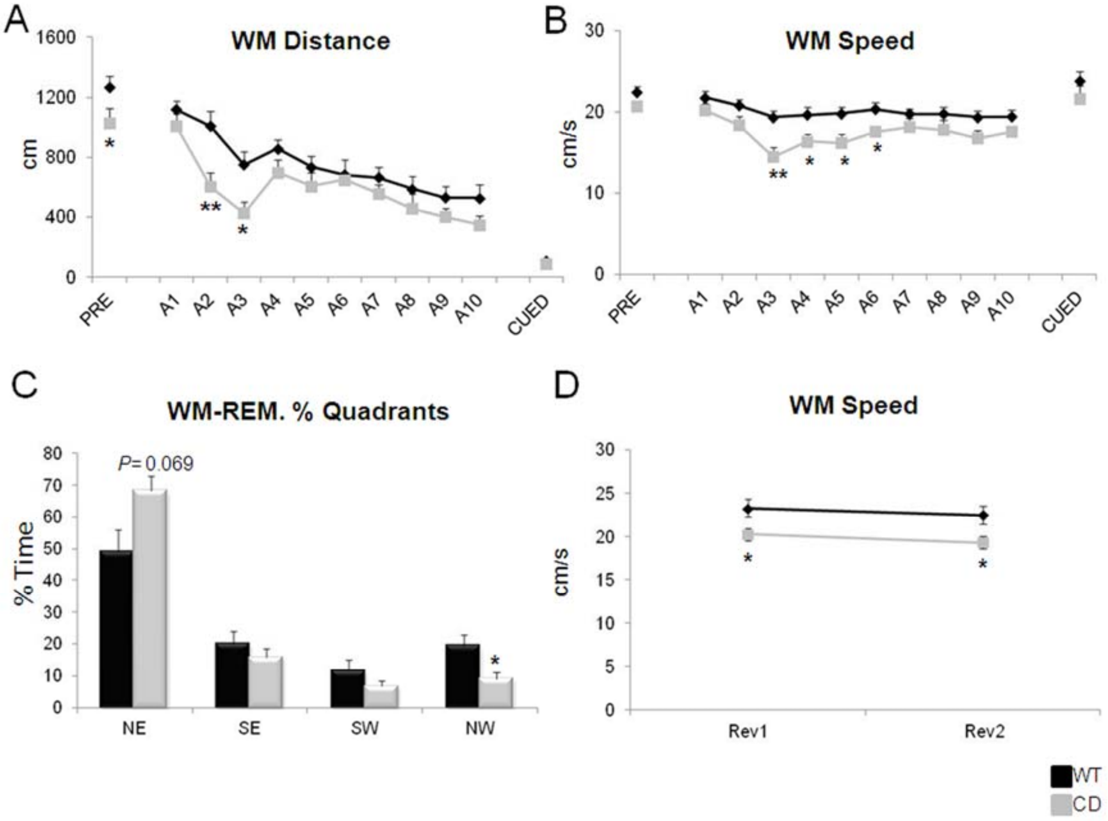
A
WM Distance
cm
1600
1200
800
400
0
*
**
*
PRE
A1
A2
A3
A4
A5
A6
A7
A8
A9
A10
CUED
B
WM Speed
cm/s
30
20
10
0
**
*
*
*
PRE
A1
A2
A3
A4
A5
A6
A7
A8
A9
A10
CUED
C
WM-REM. % Quadrants
% Time
80
70
60
50
40
30
20
10
0
P= 0.069
*
NE
SE
SW
NW
D
WM Speed
cm/s
30
25
20
15
10
5
0
*
*
Rev1
Rev2
WT
CD

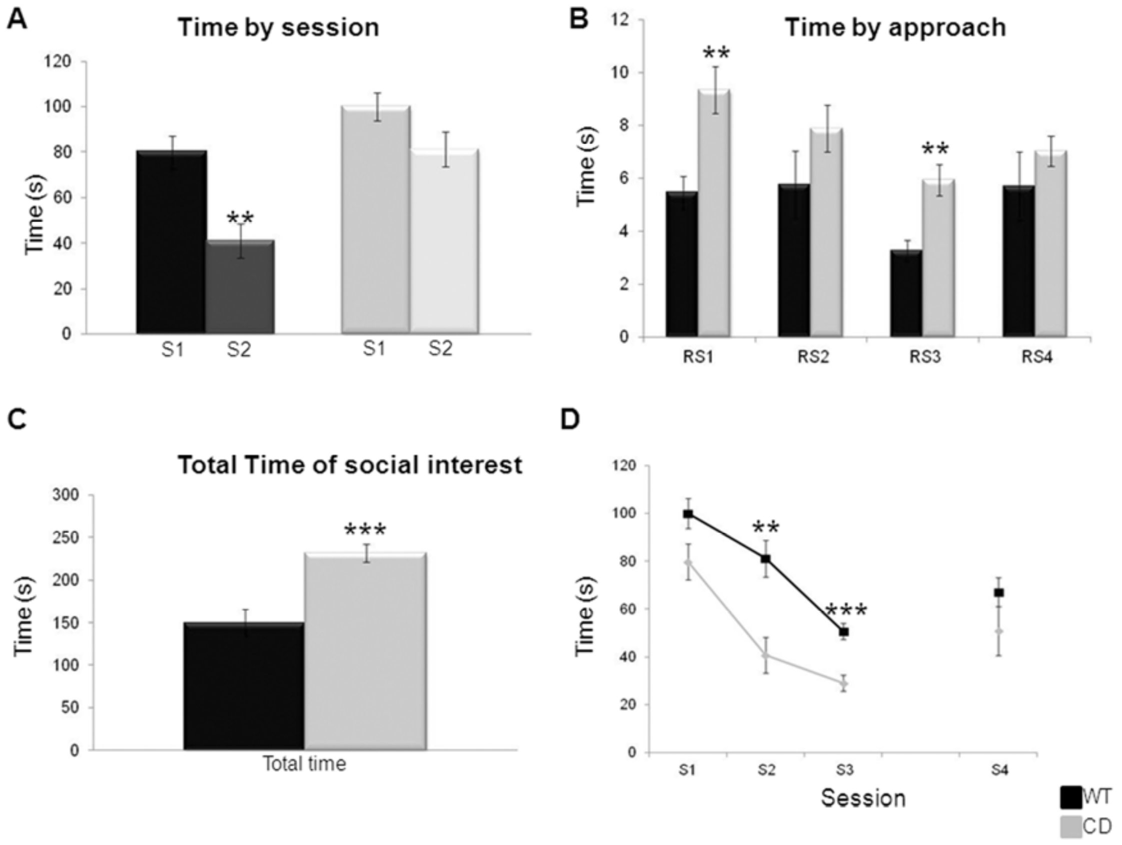
A
Time by session
Time (s)
120
100
80
60
40
20
0
**
S1
S2
S1
S2
B
Time by approach
Time (s)
12
10
8
6
4
2
0
**
**
RS1
RS2
RS3
RS4
C
Total Time of social interest
Time (s)
300
250
200
150
100
50
0
***
Total time
D
Time (s)
120
100
80
60
40
20
0
**
***
S1
S2
S3
S4
Session
WT
CD